A New and Efficient Hybrid Model for Estimating Space Diversity in Indoor Environment

J. H. Tarng, Ruey-Shan Chang, Jiunn-Ming Huang, and Yih-Min Tu

***Abstract*—This study presents a novel hybrid model based on a two-dimensional (2-D) site-specific model and a statistical model to investigate space diversity in indoor environments. The statistical model describes the field scattered by rough surface boundaries and randomly positioned scatterers, which may be important when one or both of the receiving and transmitting antennas are close to the boundaries of the scatterers. Comparing the computed spatial correlation with the measured one with the transmitting frequency at 2.44 GHz at many different sites demonstrates the effectiveness of the hybrid model. In addition to accurately predicting field strength, the hybrid model can quantify the relative mean contribution of diffused scattering in an indoor environment with a factor r. The factor is equal to the ratio of ensemble average of a randomly scattered envelope to the spatially averaged envelope. Its optimum value is in a narrow range from 0.3 to 0.5 when the intensity fluctuation at the measurement sites is in or close to saturation regions, where a large number of micromultipaths are generated. This finding confirms the relative ease in applying the hybrid model. Experimental results suggest that choosing $r = 0.4$ in a saturation allows the hybrid model to yield a satisfactory performance, as confirmed by a blind test. Moreover, good diversity gains can be obtained with an antenna spacing greater than or equal to one wavelength. Our results further demonstrate that the diversity gain of horizontally spaced antennas exceeds that of vertically spaced antennas.**

***Index Terms*—Field strength measurement, indoor environment, multipath fading, radio propagation model, space diversity.**

I. Introduction

RADIO propagation in indoor environments has received extensive interest in recent years because WLAN and PCS systems, using the UHF band as a basis, have been applied inside large office buildings [1]–[14]. Characteristics of the indoor propagation channel must be further explored to provide a reasonable cell coverage and to quantify their capacity for supporting wireless digital communication as well. Therefore, related works have developed models for narrow-band and wide-band pulse transmissions [4]–[14] in a complicated indoor environment. A phenomenon commonly known as multipath fading may seriously influence both transmissions since the transmitted signal will be experienced by different propagation modes such as reflection, refraction, diffraction, and scattering by objects and individuals such as the surrounding structures, furniture, and personnel, ultimately reaching the receiver by more than one path. Multipath fading seriously degrades the performance of a communication system operating inside buildings. Unfortunately, multipath disturbance is nearly impossible to eliminate. However, space diversity technique has been employed as an effective receiving method in a fast fading environment [15]–[18]. Nevertheless, the characteristics of indoor space diversity have seldom been explored using a theoretical approach [15]. The authors have used a three-dimensioned (3-D) site-specific model to characterize of indoor space diversity. According to their results, space diversity achieves significant benefits in terms of diversity gain and diversity advantages. Notably, antenna spacing of about $0.75 - 1\lambda$ is nearly sufficient for achieving optimum performance.

Having been extensively applied to predict radio propagation in indoor and outdoor environments, the site-specific model can incorporate the specific shape of streets, corridors, buildings, and rooms at a propagation site into computer programs and evaluate the signal at designated locations based on ray-tracing technique and diffraction theory [12]–[15]. Requiring a significant amount of computational time, the 3-D model attempts to give a deterministic prediction of the sector average signal at individual subscriber locations. Previous investigations seldom address the diffused reflection or scattered fields due to rough surfaces or randomly positioned scatterers. However, they may significantly contribute to the received field when one or both of the receiving and transmitting antennas are close to the scatterers or to the rough surface, where the diffuse scattering becomes a major propagation mode [12].

In light of the aforementioned developments, this paper presents a novel and efficient hybrid model to explore the average spatial envelope correlation and the space diversity gain in indoor environment. The proposed model consists of a two-dimensional (2-D) site-specific model and a scattering model. The scattering model is used to describe the diffuse scattering field due to rough surfaces and randomly positioned scatterers. Although spending much less computational time than that of the 3-D model, the 2-D site-specific model yields a poor prediction accuracy if used alone to evaluate a spatial correlation. However, the prediction accuracy increases after combining the 2-D model with the proposed scattering model, resulting in the hybrid model. For comparisons, the 3-D site-specific model, the 2-D and 3-D hybrid models have all been developed. The 2-D and 3-D hybrid models will adopt the same scattering field. The site specific models are incorporated with the building floor blueprint in numerical simulations. In addition, the proposed model employs the patched-wall model [14] to describe the floor layout in detail by using patches with different dielectric constants and sizes, thereby increasing the prediction accuracy of field strength. The scattering model

Manuscript received August 6, 1997; revised May 7, 1999. This work was supported by the National Science Council of the Republic of China, Taiwan, under Contracts NSC 86-2221-E-009-31 and NSC 87-2213-E-009-148.

The authors are with the Department of Communication Engineering, National Chiao Tung University, Hsin-Chu, Taiwan, R.O.C.

Publisher Item Identifier S 0018-9545(00)02544-5.

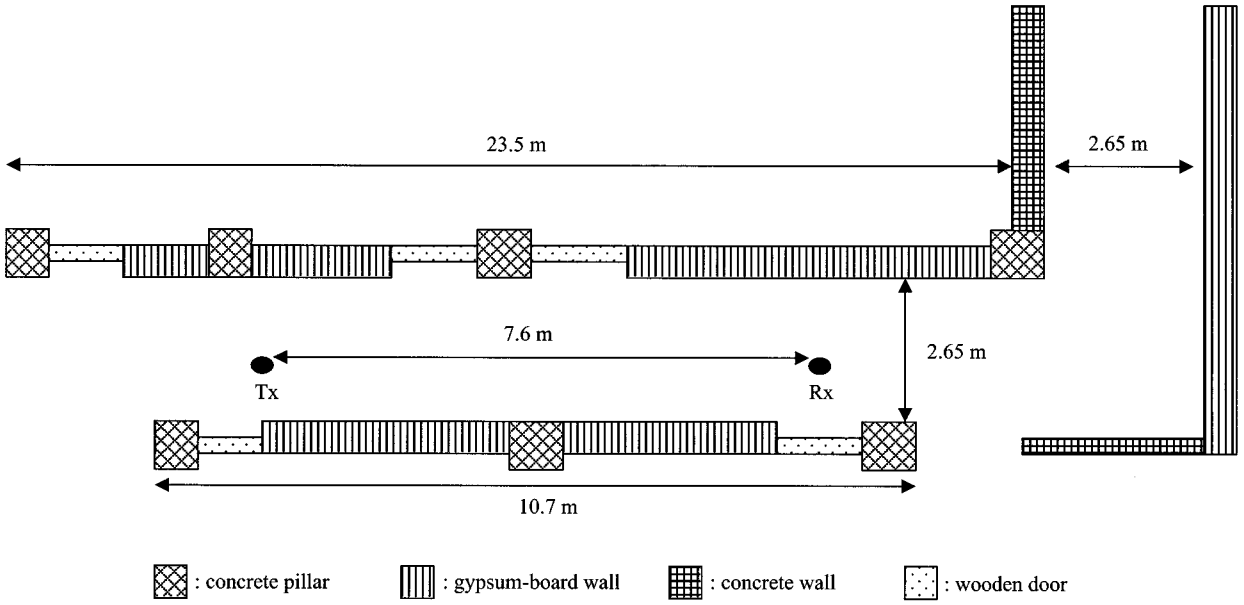

Fig. 1. Measurement site #1 is described by the patched-wall model. Tx and Rx represent the position of the transmitting and receiving antennas, respectively. Four kinds of patch are used.

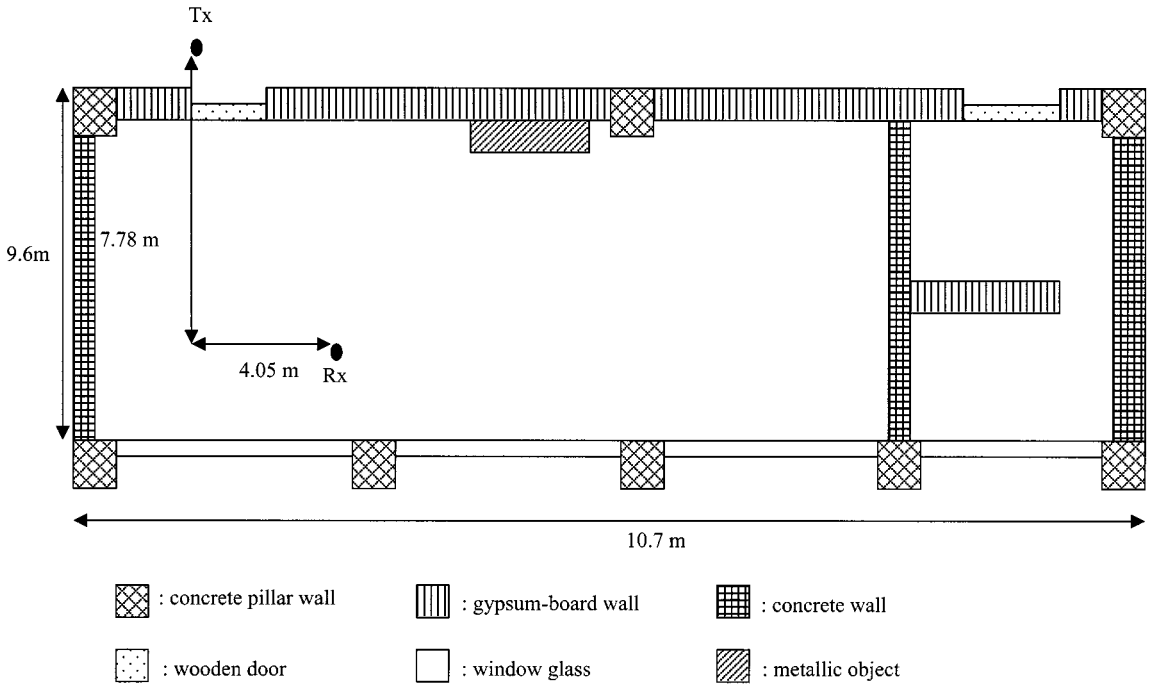

Fig. 2. Measurement site #2 is described by using six kinds of patch.

can effectively quantify the contribution of diffused scattering. Moreover, the measurement data of a 2.44-GHz radio propagating at various sites in buildings verify the computed spatial correlation.

II. Hybrid Model

In the hybrid model, the electric field after received by the antenna is determined by a superposition of deterministic and random rays. It can be expressed as

$$E_r = E_{dr} + E_{sr} \tag{1}$$

where $E_{dr} = \vec{\rho}^* \cdot \sum_i \vec{E}_{di}$ and $E_{sr} = \vec{\rho}^* \cdot \sum_i \vec{E}_{si}$ with $\vec{\rho}^*$ being the complex conjugation of unit polarization vector of the receiving antenna. E_{dr} is equal to the summation of deterministic ray fields, which are computed by a site-specific model [13], [14]. E_{sr} is a random field with zero mean, which describes the received field due to rough surface boundaries and/or randomly positioned scatterers.

A. Site-Specific Model

The 2-D site-specific model includes direct, reflected, and refracted fields and describes them by rays [13], [14]. Each propa-

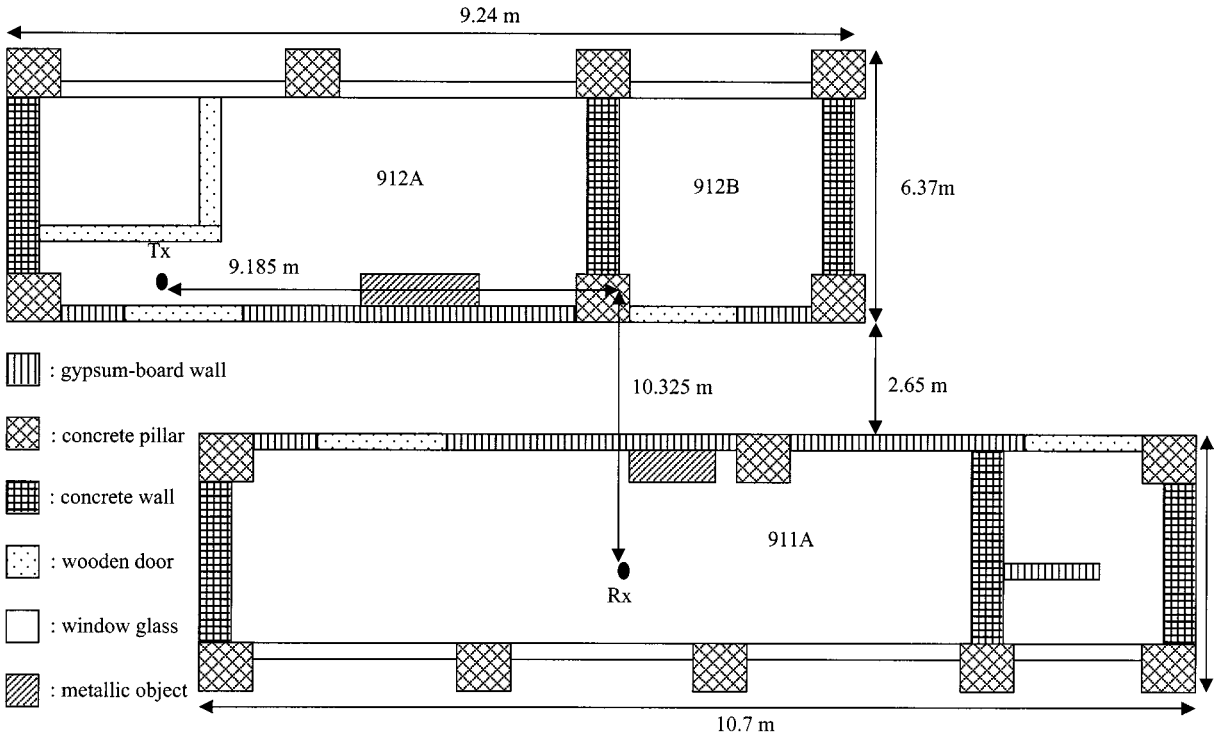

Fig. 3. Measurement site #3 is characterized by using six kinds of patch.

gation mechanism is treated separately. The complex deterministic field, E_{dr}, is given by

$$E_{dr} = \sum_i E_0 G_{ti} G_{ri} L_i(d) L_D \prod R_c(\theta_{ji}) \prod T(\theta_{mi}) \tag{2}$$

where E_0 is the field envelope 1 m away from the transmitting antenna, G_{ti} and G_{ri} are the field-amplitude radiation patterns of the transmitting and the receiving antennas, respectively, L_D is the singly diffracted loss, $L_i(d)$ is the free-space path loss of the ith ray with a unfold length d, R_c and T are the reflection and transmission coefficients, respectively, and θ_{ji} and θ_{mi} are the jth and mth reflecting and transmitting angles, respectively. Notably in the computation of the reflection or transmission coefficient, the reflecting or transmitting boundary is treated as a multilayered structure and the ABCD matrix method is used [19]. In the line-of-sight (LOS) propagation, the floor-reflected ray is also included and computed by using (2) with $T = 1$.

The tracing technique is applied to trace the significant rays from a transmitter location to a receiver location in a three dimensional space. The transmitting unit sphere is decomposed into many ray tubes. A source ray during the tracing process represents each ray tube, chosen to have a nearly equal shape and area. The tracing is accomplished by exhaustively searching using a ray tree, accounting for the decomposition of the ray at each building–object intersection. The object intersection represents a point at which an incident ray intersects with an object boundary such as wall surface and window glass. Once the intersection occurs, the ray is decomposed into reflected and transmitted (refracted) rays at the intersection and both rays are treated separately in a similar manner as a source ray. The recursion continues until either a maximum number of ray-tree levels are exceeded or no further intersections occur. Although site dependent, the maximum number of levels in the tree must be greater than the maximum number of walls crossed by the direct ray between transmitter and receivers. Herein, seven or eight levels are used to perform the simulations, resulting in converged path loss. The reception sphere is also used to determine whether or not the traced ray approaching a receiving point is received [12], [13].

B. Scattering Model

Previous investigations have proposed three models for mobile propagation environments to describe the scattered field [20], [21]. According to their results, these models are equivalent to each other as long as the total number of received rays is large enough. As is generally known, the coherence bandwidth of indoor propagation channel is normally wider than the signal bandwidth and the total number of received rays is large. Therefore, in this work, one of these models is chosen to describe the randomly scattered field inside buildings. With this chosen model, the angles of arrival were allowed to occur at random with equal probability of any direction, although the phases were completely random, and the amplitudes were assumed to be constant. Therefore, the receiving scattered field is formulated as

$$E_{sr} = E_o \sum_{n=1}^{N} \exp(j\phi_n) \tag{3}$$

where ϕ_n is a random phase which is uniformly distributed throughout 0 to 2π, N is the total number of received rays, and E_0 is an arbitrary constant. Notably, with statistical characteristics of the parameters in (3), $|E_{sr}|$ should follow a Rayleigh

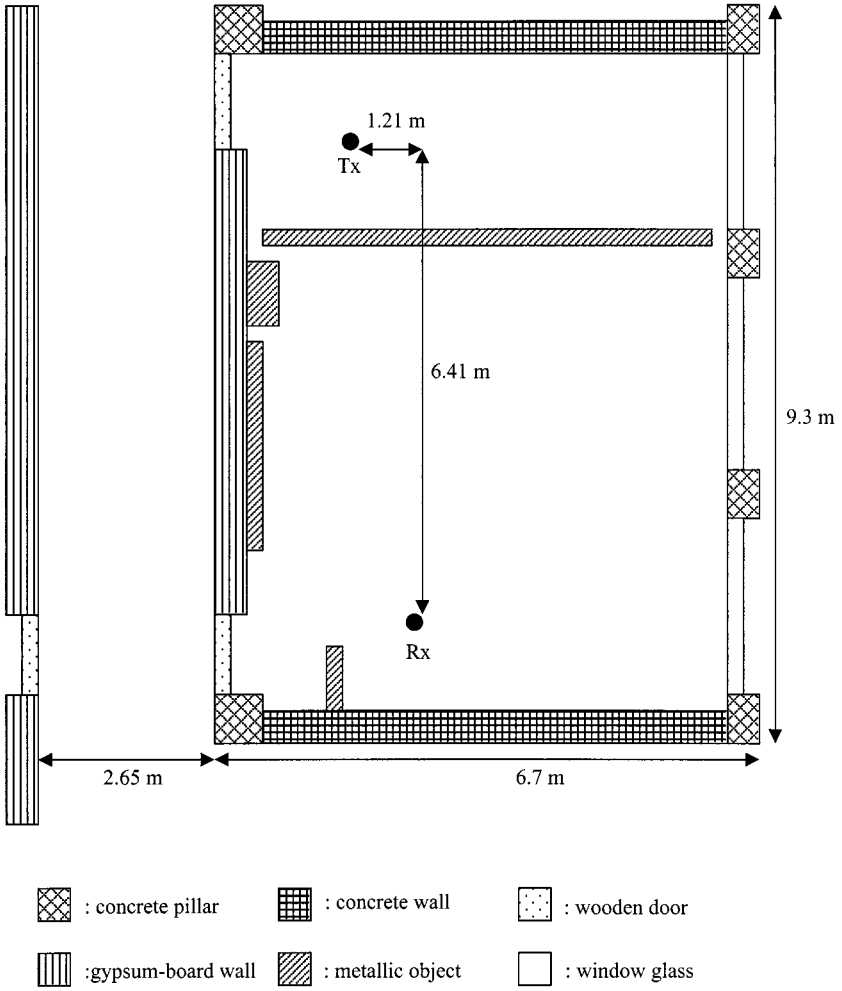

Fig. 4. Measurement site #4 with the DTR blocked by metallic bookcases.

distribution. In addition, the spatial correlation function of the scattered field can be derived and given by

$$R_{E_{sr}}(d) = \langle E_{sr}(r) E_{sr}^{*}(r+d) \rangle = N E_o^2 J_o(kd) \tag{4}$$

where $\langle \cdot \rangle$ and J_o are the ensemble average and the zero-order Bessel function of the first kind, respectively, and k and d are the free-space wavenumber and spatial distance, respectively. In addition, the relation described in (4) is used to generate the sampled scattered fields, which are correlated to each other.

III. Space Diversity Performance

Good communication quality in multipath propagation environments can be achieved by reducing the effect of deep fading, which can be achieved by diversity reception. Diversity exploits the random nature of radio propagation by finding independent (or at least highly uncorrelated) signal paths for communication. The spatial correlation of a signal can help determine the separation distance between the two-branch receivers. The envelope spatial correlation coefficient is estimated to obtain the optimum distance. It is defined as [15]

$$\rho = \frac{\langle \{ (|E_{r1}| - \langle |E_{r1}| \rangle)(|E_{r2}| - \langle |E_{r2}| \rangle) \} \rangle}{\sigma_1 \sigma_2} \tag{5}$$

where $|E_{r1}|$ and $|E_{r2}|$ are the received envelopes at branches 1 and 2, respectively, and σ_i is the standard deviation of the fading envelope in the ith branch with $i = 1$ or 2.

Next, the performance improvements in signal statistics are assessed through diversity combing. Two-branch selection, equal gain, and maximal-ratio combining technique are numerically simulated with the recorded envelopes of the two branches for each diversity scheme as inputs. Given that the received envelopes for the two branches are $|E_{r1}|$ and $|E_{r2}|$, respectively, the resultant envelope in each sample event is given by

$$E_c = \begin{cases} \max(|E_{r1}|, |E_{r2}|), & \text{for signal selection (SEL)} \\ \dfrac{(|E_{r1}| + |E_{r2}|)}{\sqrt{2}}, & \text{for equal gain combining (EGC)} \\ \sqrt{(|E_{r1}|^2 + |E_{r2}|^2)}, & \text{for maximum ratio combining (MRC).} \end{cases} \tag{6}$$

The performance of the combining techniques can be quantified in terms of diversity gain. Without a loss of generality, the gain is

obtained by comparing to the performance of branch 1 without diversity and is defined as

$$G(P_o) = 20\log_{10}\left[\frac{F_x^{-1}(P_o)}{F_1^{-1}(P_o)}\right] \tag{7}$$

where $F_x^{-1}(P_o)$ is the inverse function of the cumulative distribution functions for the fading envelope after combining. Herein, X = SEL, EGC, or MRC, P_o is the outage probability specification, and $G(P_o)$ is also an indicator of how many decibels can be saved when adopting the diversity technique for a fixed outage probability.

IV. Measurement Setup and Sites and Diversity Gain

A. Measurement Setup and Sites

Narrow-band (CW) signal strength measurements were taken at 2.44 GHz. A 13-dBm CW signal was transmitted by a half-wavelength dipole antenna at a height 1.6 m above the ground. The transmitting system, including a signal generator, a section of cable, and the transmitting antenna, was calibrated in an anechoic chamber to measure the 1-m transmitting field strength in free space. The receiving antenna is also a half-wavelength dipole antenna (Anritsu MP663A) with the same height. Both the transmitting and receiving antennas are vertically polarized during the measurement. The receiver (Advantest R3261A) can instantaneously measure the signal strength between −30 to −110 dBm over a 100-kHz interval. To ensure that the propagation channel is time stationary during the measurement, the measured data were averaged on screen over ten instantaneously sampled data. The received data were acquired automatically by a personal computer with a GPIB card.

Each measured location was associated with a $5\lambda \times 5\lambda$ square area. In this area, 21 × 21-grid subpoints were chosen and the received power was sampled at these subpoints. These subpoints were arranged in such a manner that 21 equally spaced subpoints were lined along each side of the square, i.e., λ/4 spacing between any neighboring subpoints along each side.

The four measurement sites in this study are all located on the same floor of the Engineering Building #4 at the National Chiao-Tung University, Hsin-Chu, Taiwan. Both LOS and non-line-of-sight (NLOS) measurements were taken. The measurement at site #1 (Fig. 1) is the only one with LOS propagation. At sites #2 and #3 (Figs. 2 and 3, respectively), positions of the receiving antenna were properly arranged such that the metallic objects would not block the direct-transmitted ray (DTR). At site #4 (Fig. 4), a metallic bookcase blocks the DTR. These sites are carefully chosen to include the generic propagation features and can be roughly categorized into two groups: 1) the site with light surrounding clutters such as sites #1 and #2) with heavy clutter situations such as sites #2–4.

To describe propagation environment properly, the patched-wall model [14] is employed and six kinds of patch are used, including wooden doors, gypsum-board walls, windows, pillars, concrete walls, and metallic plates. Four rectangular metallic patches are used to form the surfaces of the bookcase or the air conditioner. Metallic objects on the floor, including cabinets, bookcases, standing air conditioners, and whiteboards, are treated in the ray-tracing process since they are important reflecting articles. The concrete pillar is treated as a hollow post, and each facet is modeled as a concrete patch.

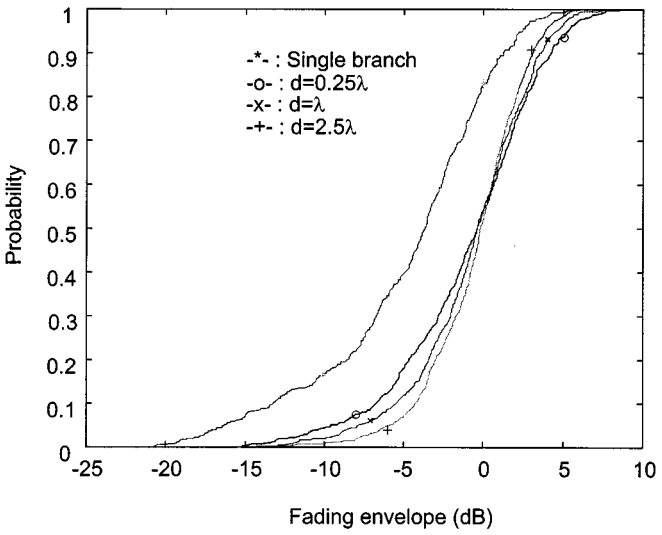

(a)

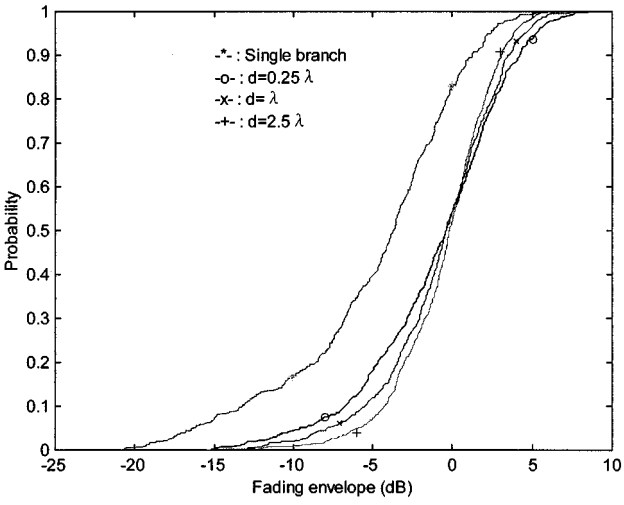

(b)

Fig. 5. Selection combining cumulative distribution for single and combining fading envelopes for different antenna spacings. (a) Site #1 and (b) site #4.

B. Diversity Gain

Experimental results of the received fading envelope at each site are used to evaluate the performance of space diversity by taking into account the linear combination of the received signals. Fig. 5(a) and (b) illustrates the cumulative distributions of selection combining for single and combining fading envelopes with different antenna spacings for sites #1 and #4, respectively. Notably, the single branch significantly improves even for antenna separations as small as separation distance $d = 0.25\lambda$. According to the experimental data as illustrated in Fig. 6(a) and (b) and (6) and (7), MRC and SEL combining techniques give the best and worst combining results, respectively. This result is similar to that in [15].

After some manipulations and $P_o = 0.01$, the horizontal diversity gain using MRC combining technique at these four sites

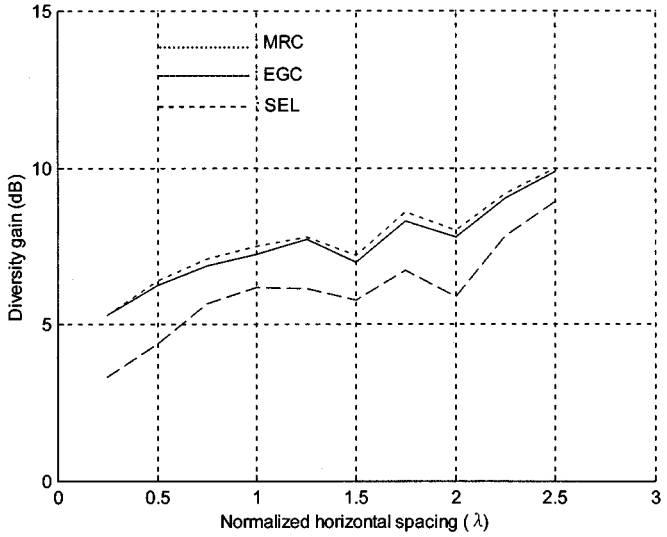

(a)

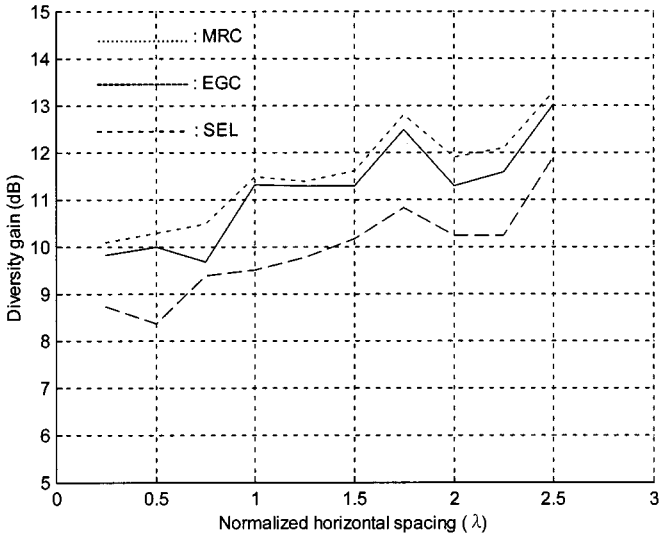

(b)

Fig. 6. The diversity gain using MRC, EGC, or SEL combining technique is illustrated as a function of normalized horizontal spacing of diversity antennas. (a) Site #1 and (b) site #4.

is illustrated in Table I. $P_o = 0.01$ implies that the received envelope is below the averaged envelope by a designated factor with 0.01 probability. This table reveals that for a fixed distance between the diversity antennas, diversity gain is larger when the site number is larger. It is because that the heavier clutter environment, such as at sites #3 or #4, leads to a lower spatial correlation, i.e., higher diversity gain. Our results further indicate that the diversity gain increases asymptotically with an increase of the separation distance between diversity antennas.

V. Comparison and Discussion

A. Validation of the Site-Specific Model

The measurement at 2.44 GHz validates the 2-D site-specific model. In the numerical simulation made with the site-specific model, 360 source rays are generated and traced. The dielectric constants of gypsum-board walls, wooden doors,

TABLE I
Value of Horizontal Diversity Gain Using MRC Combining Technique for Different Spacing Between Diversity Antennas

Antenna Spacing(λ)	Diversity Gain (dB)			
	Site No.1	Site No.2	Site No.3	Site No.4
0.25	5.3	7.0	7.8	10.1
0.50	6.4	6.8	7.9	10.3
0.75	7.1	7.3	9.8	10.5
1.00	7.5	7.8	8.6	11.5
1.25	7.8	8.1	9.9	11.4
1.50	7.2	8.2	8.7	11.6
1.75	8.6	7.8	10.2	12.8
2.00	8.0	7.6	9.8	11.9
2.25	9.2	9.7	10.4	12.1
2.50	10.0	10.2	9.4	13.3

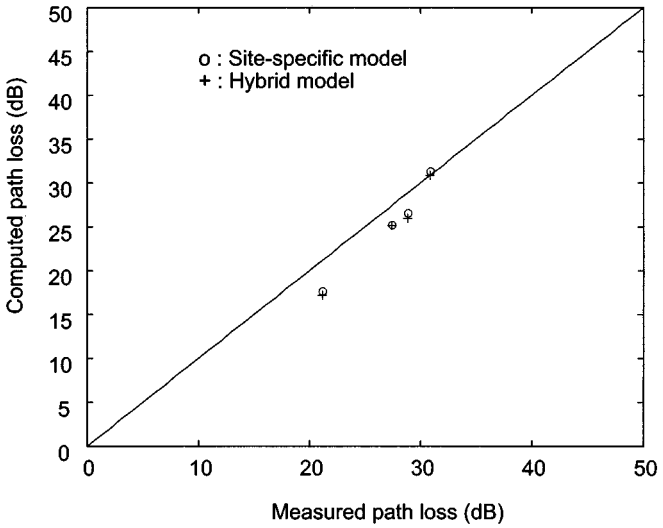

Fig. 7. A scatter plot of predicted path loss versus measured one for sites #1–4.

concrete walls, and ground floors are chosen to equal 5-0.062j, 5-0.062j, 7-0.6j, and 7-0.6j, respectively [22], [23]. Fig. 7 presents a scatter plot of computed path loss versus measured path loss at different sites. According to this figure, both the 2-D site-specific and hybrid models, which are combined with the patched-wall model, have a reasonable prediction accuracy. Since the diffuse scattering term has zero mean, the averaged path loss computed by both models is nearly the same.

B. Spatial Correlation

The discrete correlation function $C(k)$ corresponding to a discrete sampling of the field in space is defined as [15]

$$C(k) = \frac{\sum_{i=1}^{N-k} \{\omega(i) - \omega_m\}\{\omega(i+k) - \omega_m\}}{\sum_{i=1}^{N-k} \{\omega(i) - \omega_m\}^2}. \quad (8)$$

This function corresponds to a continuous spatial correlation at the normalized distance $k\Delta_S/\lambda$ with Δ_S and λ being the sampling step in space and wavelength, respectively. Herein, $\omega(i)$,

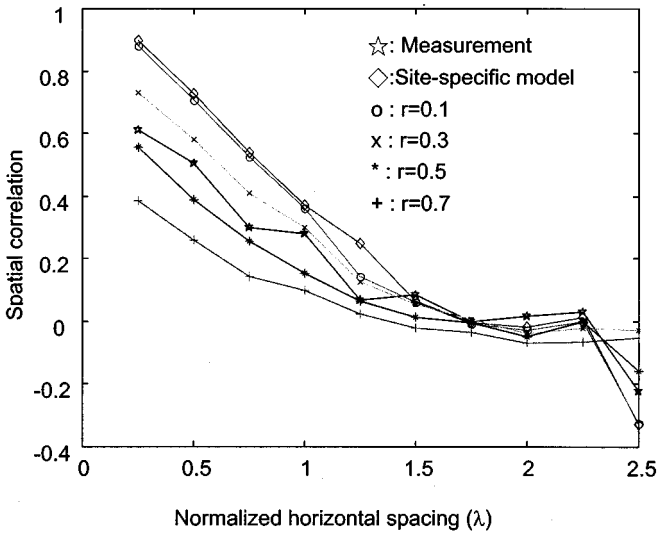

Fig. 8. The spatial correlation function is plotted as a function of the normalized horizontal spacing between diversity antennas. 2.44-GHz measured data carried out at site #1 is compared with the computed value with $r = 0.1, 0.3, 0.5,$ or 0.7.

$i = 1, \cdots, N$ can be the computed or measured envelope samples at the measured spot. In addition, ω_m is the corresponding average value.

Since the $(i+1)$th sampled complex scattered field is related to the ith sampled field, their relation can be described using the AR-1 (first-order autoregressive model) method [24]

$$E_{sr}(i+1) = E_{sr}(k)R_\rho + \sqrt{1-R_\rho^2}[N_1(0,\sigma) + jN_2(0,\sigma)] \tag{9}$$

where R_ρ is the normalized R_{Esr} and $N_1(0,\sigma)$ and $N_2(0,\sigma)$ are independent Gaussion random variables with zero mean and standard deviation σ. Since $|E_{sr}|$ follows a Rayleigh distribution, $\sigma = \sqrt{2/\pi}\langle|E_{sr}|\rangle$. Herein, the value of σ or $\langle|E_{sr}|\rangle$ is determined from the experimental data. To more easily determine σ, a factor $r = \langle|E_{sr}|\rangle/|E_{dr}|_{ave}$ is defined with $|E_{dr}|_{ave}$ being the spatially averaged deterministic envelope.

Fig. 8 illustrates the discrete spatial correlation as a function of normalized horizontal spacing (in wavelength) between diversity antennas. 2.44-GHz measured data at site #1 is compared with the predicted data. That comparison reveals that the hybrid model and the 2-D site-specific model yield a reasonable prediction accuracy. In this figure, the former model with $r = 0.1, 0.3, 0.5,$ and 0.7 is used to predict the spatial correlation. The hybrid model, including randomly scattered fields, yields a better prediction accuracy than that of the 2-D site-specific model with a properly chosen value of r.

To determine the optimum value of r, the root mean square error of the spatial correlation, $\sigma_{s.c.}$, is defined to quantify the prediction accuracy of the hybrid model. When the mean of $\sigma_{s.c.}$ is minimized, optimum r is obtained. Fig. 9 displays four curves to describe how the mean of $\sigma_{s.c.}$ being changed as r is varied at each site with individual propagation scenarios. Interestingly, the mean of $\sigma_{s.c.}$ is minimized when the value of r is confined in a narrow range from 0.3 to 0.5, which is true for these four

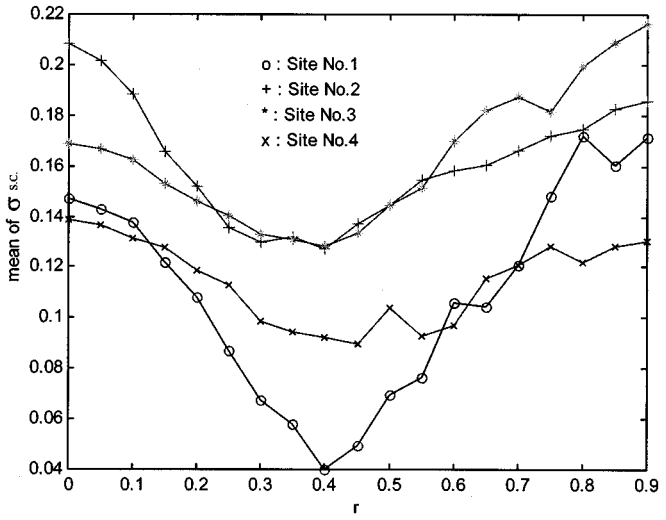

Fig. 9. Mean of $\sigma_{s.c.}$ is illustrated as a function of r to determine the optimum value of r.

TABLE II
VALUE OF $\sigma_{s.c.}$ FOR 2-D SITE-SPECIFIC AND HYBRID MODELS AT SITES #1–4

Site Number	$\sigma_{s.c.}$	
	2-D site-specific model	2-D hybrid model(r=0.4)
No.1	0.1473	0.0400
No.2	0.2082	0.1273
No.3	0.1688	0.1282
No.4	0.1387	0.0922

TABLE III
VALUE OF $\sigma_{s.c.}$ FOR 2-D SITE-SPECIFIC AND HYBRID MODELS AT SITES #5–8

Site Number	$\sigma_{s.c.}$	
	2-D site-specific model	2-D hybrid model(r=0.4)
No.5	0.2144	0.1310
No.6	0.1488	0.1014
No.7	0.2800	0.1071
No.8	0.2477	0.1477

measurement sites. According to Fig. 9, this narrow range includes all the lowest mean values of $\sigma_{s.c.}$ for these four sites. It implies that our hybrid model can effectively quantify the relative contribution of diffused scattering in an indoor environment by setting r equal to a value choosing from range of (0.3, 0.5). To validate this argument, first, the computed spatial correlation choosing $r = 0.4$, the center value of range (0.3, 0.5), is compared with the measured one. The comparisons are made at sites #1–4 in which Table II summarizes those results. According to this table, the hybrid model with $r = 0.4$ works better than the 2-D site-specific model. Second, measurements are taken at the other four sites (#5–8) in the same building to make a blind test of the hybrid model by choosing $r = 0.4$. For conciseness, layouts of these sites are not illustrated. Although the experiment of LOS propagation is conducted at site #5, the experiment of NLOS propagation is conducted at the three other sites. Table III presents the root mean square error of the spatial correlation for these four sites. According to this table, the hybrid model with $r = 0.4$ has a better performance than the site-specific model in terms of estimating the spatial correlation.

TABLE IV
VALUE OF $\sigma_{s.c.}$ FOR 3-D SITE-SPECIFIC MODEL AND 2-D AND 3-D HYBRID MODELS

Site Number	$\sigma_{s.c.}$		
	2-D hybrid model(r=0.4)	3-D site-specific model	3-D hybrid model(r=0.4)
No.1	0.0400	0.1437	0.1126
No.2	0.1273	0.2990	0.1766
No.4	0.0922	0.1882	0.1065
No.5	0.1306	0.1332	0.1142
No.6	0.0883	0.1200	0.0744
No.7	0.1079	0.1741	0.0778

Table IV summarizes $\sigma_{s.c.}$ of sites #1, #2, and #4–7. For comparison, the 3-D site-specific model and the 2-D and 3-D hybrid models are used. [14] described in detail the formulation of the 3-D site-specific model. Interestingly, both hybrid models always yield a better performance or smaller $\sigma_{s.c.}$ than that of the site-specific model. In contrast, the 3-D hybrid model does not always yield a smaller $\sigma_{s.c.}$ than that of the 2-D hybrid model, for example, $\sigma_{s.c.}$ at sites #1, #2, and #4. With its superior performance in terms of prediction accuracy and computational efficiency, the 2-D hybrid model is efficient in terms of predicting space diversity.

To validate the applicability of the 2-D hybrid model, the model is verified by the measured data acquired at other five sites (#9–13). These sites are located at the other three buildings on campus, which are Engineering Building #3, Science Building #2, and the Chung-Cheng Auditorium. Sites #9 and #10 are located at a computer room in Engineering Building #3. The room is filled with computers and furniture: its layout is illustrated in Fig. 10. It is a heavily cluttered environment. Both LOS and NLOS measurements are performed. Sites #11 and #12 located in Science Building #2 have layouts similar to the previous sites and, therefore, are not illustrated herein. Fig. 11 shows site #13, the lobby of the Auditorium, which has a large empty space (19.7 m × 11.7 m × 12 m) with slightly rough walls. It is a site with light surrounding clutters. Table V presents the $\sigma_{s.c.}$ for sites #9–13 with the 2-D hybrid model and the 2-D site-specific model being used. According to this table, the hybrid model still has a better performance than the 2-D site-specific model, particularly at a heavy clutter environment such as at sites #9 and #10.

C. Discussion

The aforementioned comparisons reveal that the hybrid model, which includes the diffuse scattering contribution, can enhance the estimation accuracy of the spatial correlation with a proper choice of factor r. The factor is confined to a narrow range when the intensity fluctuation at these sites is in or close to saturation regions, where a large number of micromultipaths (multipath due to diffuse scattering) are generated [25]. In the regions, the value of the scintillation index is close to or more than unity [25], [26]. The index is a parameter to measure the variance of the signal intensity, which is defined by $\sigma_1^2 = (\langle I^2\rangle - \langle I\rangle^2)/\langle I\rangle^2$ with I being the field intensity. Notably, measured values of σ_I^2 at sites #1–4 are equal to 0.98, 0.73, 1.44, and 0.71, respectively, which are all close to or more than one. Therefore, the ratio

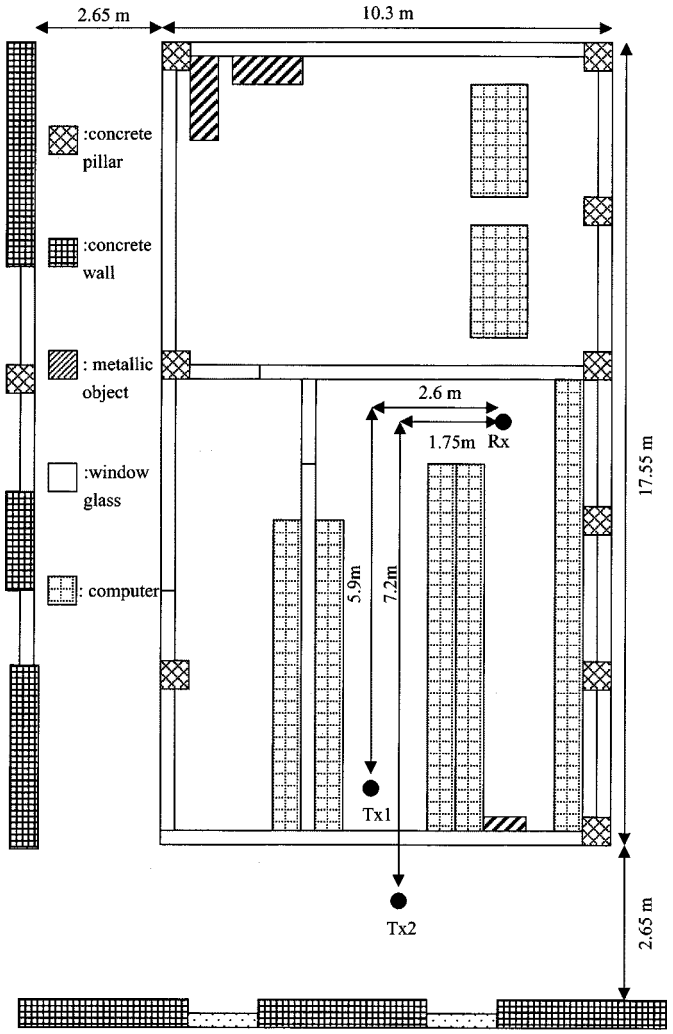

Fig. 10. Floor layout of measurement sites #9 (Tx1-Rx) and #10 (Tx2-Rx).

of the ensemble average of randomly scattered envelope to the spatially averaged deterministic envelope fluctuates in a narrow range in saturation regions. Notably, when the intensity fluctuation is in an unsaturated region, i.e., σ_I^2 is not close to unity, optimum value of r may not be confined in range (0.3, 0.5). For example, optimum value of r is equal to 0.2 for site #13 and yields $\sigma_{s.c.} = 0.055$. It is a site with light surrounding clutters in which the measured σ_I^2 is equal to 0.46.

Fig. 12 illustrates how the spatial correlation value changes as r is varied at sites #1–4. According to this figure, the correlation coefficient decreases asymptotically with an increase of r at sites #1, #2, and #4. It implies that the larger the r implies a larger diffused scattering contribution, leading to a lower correlation between sampled envelopes. However, the value of r oscillates as the coefficient approaches zero such as the case at site #3.

VI. CONCLUSION

This work presents a novel and efficient hybrid model to estimate the spatial correlation for the use of space diversity in indoor environments. The hybrid model, which combines a site-specific 2-D model and a scattered model, yields a better

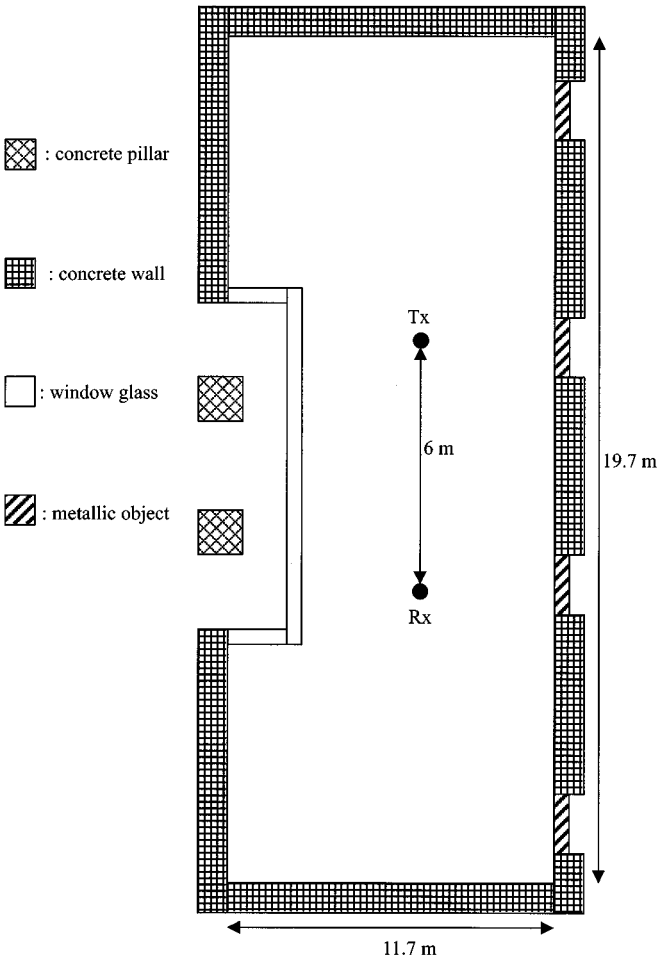

Fig. 11. Floor layout of measurement site #13: the lobby of the Chung-Cheng Auditorium.

TABLE V
VALUE OF $\sigma_{s.c.}$ FOR 2-D SITE-SPECIFIC AND HYBRID MODELS AT SITES #9–13

Site Number	$\sigma_{s.c.}$	
	2-D site-specific model	2-D hybrid model(r=0.4)
No.9(NLOS)	0.3124	0.1002
No.10(LOS)	0.2884	0.1150
No.11	0.1473	0.0918
No.12	0.1588	0.1032
No.13	0.1488	0.1154

estimation accuracy on the spatial correlation than that of the 2-D deterministic model. This improved accuracy is confirmed by comparing the computed data with the measured data at eight different sites. The proposed hybrid model not only enhances the prediction accuracy, but also properly quantifies the mean of relative contribution of diffuse scattering with a properly chosen factor r. According to our study and the experimental result, value of r fluctuates in a narrow range from 0.3 to 0.5 for saturation regions. In this region, a large number of micromultipaths are generated and the received strength or scintillation index is close to or more than one. It seems that this situation happens quite often at indoor environments. In unsaturation regions such as propagation in an empty, open space indoor scenario, the value of r is in a different range from 0.05 to 0.02. Notably, there

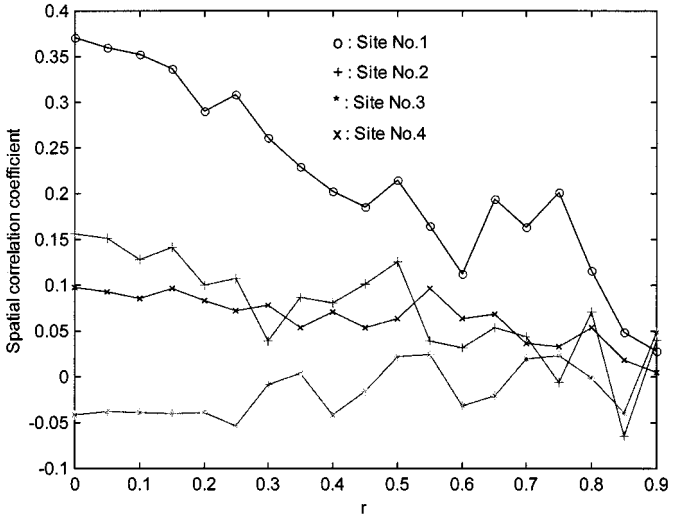

Fig. 12. The spatial correlation function is plotted as a function of r.

TABLE VI
VALUE OF VERTICAL DIVERSITY GAIN USING MRC COMBINING TECHNIQUE FOR DIFFERENT SPACING BETWEEN DIVERSITY ANTENNAS

Antenna spacing (λ)	site No.1	Diversity site No.2	Gain (dB) site No.3	site No.4
0.5	5.7	6.0	6.3	8.8
1.0	6.7	6.8	8.5	9.8
1.5	7.0	7.3	9.4	11.7
2.0	7.9	8.2	10.5	12.2
2.5	8.1	8.4	10.8	13.3
3.0	8.3	8.4	11.1	13.8

is no strict line to distinguish these two regions. Further study will be conducted in the near future to examine this issue more closely with more experimental data. The measurement sites chosen herein include both LOS and NLOS propagation with, at most, two partitions between the transmitting and receiving antennas. The distance between these two antennas ranges from 5 to 15 m. Our results further indicate that good diversity gains can be obtained with antenna spacing greater than or equal to one wavelength.

This work focuses mainly on horizontal diversity. However, studying vertical diversity would also be an interesting topic. According to our experimental data on vertical diversity (Table VI), the vertical diversity gain is smaller than that of the horizontal one as the diversity antennas having an equal separation distance in the same environment. It implies that with the same antenna, spacing correlation of horizontal separation is smaller than that of vertical separation. This discrepancy is due to the fact that the propagation paths before arrival at any two horizontally separated points may undergo an environmental change more rapidly than those of vertically separated points. For example, the major propagation boundaries in the horizontal plane, as formed by metallic object and interior walls or partitions, change more rapidly than those in the vertical plane, which are formed by uniform structures such as ceilings or floors. Our study in the near future will investigate whether

or not the proposed hybrid model can be effectively applied to estimate the vertical spatial correlation.

REFERENCES

[1] M. Marcus, "Regulatory policy consideration for radio local area networks," *IEEE Commun. Mag.*, vol. 25, no. 7, pp. 95–99, 1987.

[2] H. Hashemi, "The indoor radio propagation channel," *Proc. IEEE*, vol. 81, no. 7, pp. 943–968, 1993.

[3] D. Molkdar, "Review on radio propagation into and within buildings," *Proc. Inst. Elect. Eng.*, vol. 138, pt. H, pp. 61–73, Feb. 1991.

[4] A. Kajiwara, "Line-of-sight indoor radio communication using circular polarized waves," *IEEE Trans. Veh. Technol.*, vol. 44, no. 3, pp. 487–493, 1995.

[5] R. Bultitude, S. Mahmoud, and W. Sullivan, "A comparison of indoor radio propagation characteristics at 910 MHz and 1.75 GHz," *IEEE J. Select. Areas Commun.*, vol. 7, pp. 20–30, Jan. 1989.

[6] J. F. Lafortune and M. Lecours, "Measurement and modeling of propagation losses in a building at 900 MHz," *IEEE Trans. Veh. Technol.*, vol. 39, no. 2, pp. 101–108, 1990.

[7] S. Y. Seidel and T. S. Rappaport, "Path loss prediction in multifloored buildings at 914 MHz," *Electron. Lett.*, vol. 27, pp. 1384–1387, July 1991.

[8] A. J. Motley and J. M. P. Keenan, "Personal communication radio coverage in buildings at 900 MHz and 1700 MHz," *Electron. Lett.*, vol. 24, pp. 763–764, June 1988.

[9] ——, "Radio coverage in buildings," *Br. Telecom Technol. J., Special Issue Mobile Commun.*, vol. 8, pp. 19–24, 1990.

[10] A. A. M. Saleh and R. A. Valenzuela, "A statistical model for indoor multipath propagation," *IEEE J. Select. Areas Commun.*, vol. SAC-5, pp. 138–146, Feb. 1987.

[11] S. C. Kim, H. C. Bertoni, and M. Stern, "Pulse propagation characteristics at 2.44 GHz inside buildings," *IEEE Trans. Veh. Technol.*, vol. 45, no. 3, pp. 579–592, 1996.

[12] W. Honcharenko, H. L. Bertoni, J. L. Dailing, J. Qian, and H. D. Yee, "Mechanisms governing UHF propagation on single floors in modern office buildings," *IEEE Trans. Veh. Technol.*, vol. 41, pp. 496–504, 1992.

[13] S. Y. Seidel and T. S. Rappaport, "Site-specific propagation prediction for wireless in-building personal communication system design," *IEEE Trans. Veh. Technol.*, vol. 43, no. 4, pp. 879–892, 1994.

[14] J. H. Tarng, W. R. Chang, and B. J. Hsu, "Three-dimensional modeling of 900-MHz and 2.44-GHz radio propagation in corridors," *IEEE Trans. Veh. Technol.*, vol. 46, no. 2, pp. 519–527, 1997.

[15] G. E. Corazza, V. Degli-Esposti, M. Frullone, and G. Riva, "A characterization of indoor space and frequency diversity by ray-tracing modeling," *IEEE J. Select. Areas Commun.*, vol. 14, no. 3, pp. 411–419, 1996.

[16] G. A. Kalivas, M. El-Tanany, and S. Mahmoud, "Millimeter-wave channel measurements with space diversity for indoor wireless communication," *IEEE Trans. Veh. Technol.*, vol. 44, no. 3, pp. 494–505, 1995.

[17] W. C. Y. Lee, "Effects of correlation between two mobile radio base station antennas," *IEEE Trans. Commun.*, vol. COM-21, no. 11, pp. 1214–1224, 1973.

[18] A. M. D. Turkmani, A. A. Arowojolu, P. A. Jefford, and C. J. Kellett, "An experimental evaluation of the performance of two-branch space and polarization diversity schemes at 1800 MHz," *IEEE Trans. Veh. Technol.*, vol. 44, no. 2, 1995.

[19] A. Ishimaru, *Electromagnetic Wave Propagation, Radiation, and Scattering*. Englewood Cliffs, NJ: Prentice-Hall, 1991.

[20] E. N. Gilbert, "Energy reception for mobile radio," *Bell Syst. Tech. J.*, vol. 4, no. 8, pp. 1779–1803, 1965.

[21] R. H. Clarke, "A statistical theory of mobile-radio reception," *Bell Syst. Tech. J.*, vol. 47, pp. 957–1000, 1968.

[22] C. F. Yang, C. J. Ko, and C. J. Chen, "Measurement of the dielectric constants of the walls in building," in *Proc. 1st Radio Science Symp.*, Kaohsiung, Taiwan, 1995, pp. 63–67.

[23] M. C. Lawton and J. P. McGeehan, "The application of a deterministic ray launching algorithm for the prediction of radio channel characteristic in small-cell environments," *IEEE Trans. Veh. Technol.*, vol. 43, no. 4, pp. 966–969, 1994.

[24] J. E. Berg, R. Bowds, and F. Lotse, "Path loss and fading models for microcells at 900 MHz," in *Proc. VTC*, 1992, pp. 666–671.

[25] S. M. Flatte, *Sound Transmission Through a Fluctuating Ocean*. New York: Cambridge Univ., 1979.

[26] A. Ishimaru, *Wave Propagation and Scattering in Random Media*. New York: Academic, 1978.

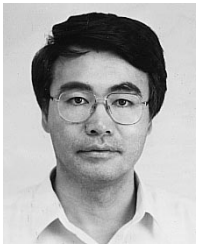

J. H. Tarng received the B.S. degree in power mechanical engineering from National Tsin-Hua University, Hsin-Chu, Taiwan, R.O.C., in 1981 and the M.S. and Ph.D. degrees in electrical engineering from Pennsylvania State University, University Park, in 1988 and 1989, respectively.

He is currently a Faculty Member in the Department of Communication Engineering, National Chiao Tung University, Hsin-Chu. His research interests include radio propagation modeling and measurement, channel assignment, and smart antenna systems.

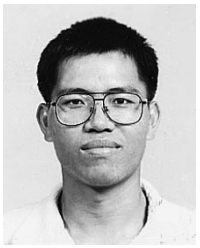

Ruey-Shan Chang received the B.S. degree in electrical engineering from Yuan-Ze University, Taiwan, R.O.C., and the M.S. degree in communication engineering from National Chao Tung University, Hsin-Chu, Taiwan, in 1996 and 1998, respectively.

His research interests are in radio propagation modeling and communication systems.

Jiunn-Ming Huang was born in Changhua, Taiwan, R.O.C. He received the B.Ed. degree from the National Changhua University of Education, Changhua, Taiwan, in 1985 and the M.Sc. degree from the Chung Chen Institute of Technology, Taoyuan, Taiwan, in 1987. He is currently working towards the Ph.D. degree at National Chiao Tung University, Hsinchu, Taiwan.

From 1987 to 1993, he was with the Chung Shan Institute of Science and Technology (CSIST), Taoyuan, working on antenna design and RCS measurements. From 1994 to 1996, he was a Consultant on mobile antennas, amateur radio, and RF circuit design. His current interests include wavelets theory in scattering, computational electromagnetics, and modem design.

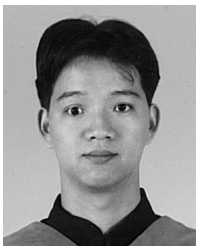

Yih-Min Tu received the B.S. degree in physics from the National Sun Yat Sen University, Taiwan, R.O.C., and the M.S. degree in communication engineering from the National Chao Tung University, Hsin-Chu, Taiwan, in 1994 and 1997, respectively.

His research interests are in radio propagation modeling and measurement for indoor radio communication.